The 9th European Congress on Computational Methods in Applied Sciences and Engineering
ECCOMAS Congress 2024
3–7 June 2024, Lisboa, Portugal

# ON THE USE OF REPRESENTATIVE INHOMOGENEOUS POISSON-VORONOI TESSELLATIONS FOR BRITTLE FRAGMENTATION MODELLING

**J. LHONNEUR**[1]

[1] Institute for Radiation Protection and Nuclear Safety (IRSN)
BP 17 - 31, avenue de la Division Leclerc, 92262 Fontenay-aux-Roses Cedex, France
e-mail: joffrey.lhonneur@irsn.fr, www.irsn.fr

**Key words:** Voronoi Tessellations, Particle size distribution, Geometric Fragmentation Statistics, Crack density

**Summary.** *The intense fragmentation of brittle radioactive solids resulting from dynamic loadings can lead to the production of airborne fragments whose dispersion in the environment has to be predicted for crisis management purposes. Numerous fragmentation models based on Mott's theory estimate crack density fields inside broken solids. However, the use of this data for estimating a fragment size distribution is not straightforward. A known method consists into choosing an algorithm to partition the solids into random fragments sets while ensuring the obtaining of crack networks associated with given crack densities. The accuracy of a fragment size distribution estimate depends then on the aptitude of the algorithm to generate fragments close to real ones in terms of size and shape.*

*In this paper, we focus our interest on the use of isotropic inhomogeneous Poisson-Voronoi tessellations to represent fragmented solids. Estimates are proposed and verified for the probability density function of the Voronoi cell size associated to a given crack density field. They are used for retrieving the cumulative fragments mass fraction observed on two ceramic tiles fragmented by edge-on-impact tests. Finally, the usage limits and outlooks of this work are presented.*

## 1 INTRODUCTION

The French Institute for Radiation Protection and Nuclear Safety (IRSN) aims to provide estimates of radiological hazards induced by accidental events or malevolent attacks involving nuclear or radioactive materials. In this framework, the airborne release and dispersion of submillimeter radioactive material particles is a topic of major interest.[1,2] The consequences associated to such a scenario strongly depend on the particle size distribution[3,4] whose estimation can be challenging. It is particularly the case when these particles correspond to radioactive material fragments induced by malevolent attacks (ballistic impacts or explosions). This statement has motivated the creation of a research program aiming at developing a numerical tool for estimating fragment size distributions resulting from the fragmentation of brittle solids.

The estimation of fragment size distributions is a key issue in numerous engineering sciences as it can be used, for example, to improve mining processes efficiency,[5–8] to study military defensive devices[9,10] or to assess explosive munitions performances.[11,12] As a consequence, various methods are proposed in literature for estimating fragment size distributions among which the

most cited are empirical methods.[1,12–15] These methods gives satisfactory results when studying well-defined scenarii for which only an estimate of an average fragment size is required, the distribution shape being generally fixed and known from direct experimental observations. However, their use is restricted to specified cases which seldom correspond to subjects of interest for the IRSN. This issue is overcome by considering mechanics-based approaches allowing for a finite element analysis of any scenario. The modelling of a crack network evolution is either carried out by considering *Surface Fracture* methods (e.g. Discrete Element Method[16] or Cohezive-Volumetric Finite Element Method[17]) or *Continuum Damage Mechanics (CDM)*-based methods.[5,6,18–24]

*Surface Fracture* methods permit modelling individually each crack initiation and propagation as well as each fragment formation. However, the computed fragments being composed of at least one elementary component of a spatial discretization of the domain of interest, an artificial *minimum fragment size* is imposed. The obtention of the whole fragment size distribution requires thus to consider a spatial discretization whose characteristic length is less than the one of the smallest expected fragment. These methods reach then their limit when studying the fragmentation of large objects into a huge quantity of small fragments. This is typically the case in most of the problems of interest for the IRSN.

For that reason, the use of *Continuum Damage Mechanics (CDM)* models seems more appropriate. Indeed, these models provide a physical framework for studying the effects of multiple cracking or voidage taking place in volume of materials smaller than finite element ones.[25] However, in contrast to *Surface Fracture* models, only a partial description of a local crack network is obtained as cracks are not individually described. The estimation of a fragment size distribution from the results of a *CDM* simulation is thus more challenging.

Most of the *CDM*-based models are derived from Mott's theory[5,6,12,18–24] which allows for estimating the evolution of the *crack density* in unidimensional solids subjected to a homogeneous tensile straining as well as the associated fragment size distribution. In turn, in each of these models the description of the fragmentation state of a solid is restricted to an estimate of a crack density field. However, retrieving a fragment size distribution from the knowledge of this data alone is not straightforward and constitutes a *Geometric Fragmentation Statistics* problem.[12–14] Indeed, a same crack density field over a given solid can be obtained by considering various partitioning algorithms associated to distinct fragment size distributions. For a partition algorithm to give an accurate estimation of a fragment size distribution, it must produce fragments whose geometrical features are representative of real ones.

Among the most known partitioning algorithms are the Voronoi tessellations. Many results have been provided on these tessellations as they are used in numerous fields such as image morphing, volume and surface mesh generation and surface representation.[26] The statistics of the cells of a Voronoi tessellation can be modified for example by selecting inhomogeneous point processes for the generation of the cell seeds or by choosing anisotropic metrics for the cell boundaries computation.[26–28] In turn, the Voronoi tessellations can reproduce numerous fragmentation patterns.

The present work focuses on inhomogeneous Poisson-Voronoi tessellations. The euclidean metric is used for computing the Voronoi tessellations. A first section presents a method for estimating fragment size distributions derived from the pioneering works of Lienau and Mott which combines the knowledge of a crack density inside a broken solid with the use of a volume partitioning algorithm. Known results on Poisson-Voronoi tessellations are presented on the next section in view of using them as partitioning algorithms. An estimate of the inhomogeneous

Poisson-Voronoi cell size probability density function is then proposed. It requires a crack density field which could be provided for example by a *CDM* model based on Mott's theory. This estimate is validated and used for estimating the cumulative mass fragment distribution of two fragmented ceramic tiles. A comparison is then made between these estimations and actual experimental measurements. Finally, a limitation on the use of this estimate is presented.

## 2 Crack density field and Geometric Fragmentation Statistics

A well-known academic result on fragmentation statistics of brittle solids was brought by the work of Lienau[29] who studied the random fragmentation of a rod subjected to a homogeneous tensile strain. He observed that experimental fragment size distributions can be accurately estimated by exponential laws. These laws describing the interarrival time distribution in a Poisson point process, Lienau suggested that the observed fragment size distributions are the result of the activation of flaws randomly distributed along the rod according to a homogeneous Poisson point process. Denoting by $\tau$ the number of activated flaws per unit rod length, namely the crack density, the fragment size probability density function reads:

$$\forall l \geq 0, \;\; f(l) = \tau \exp(-\tau l) \tag{1}$$

This result suggests that a fragment size distribution shape can be inferred from the knowledge of the spatial statistics of flaws positioning inside a uni-dimensional solid.

Lienau's approach has since been extended to two and three-dimensional fragmentation problems. The choice of a partitioning algorithm for retrieving a known fragment distribution is a *Geometric Fragmentation Statistics* problem.[12] As illustrated on Figure 1, a partitioning algorithm leads to a particular fragment size distribution. In most cases, the tessellations obtained by these algorithms are entirely described by one parameter, for example a fragment density or a Point-process density, which permits selecting an average fragment size.

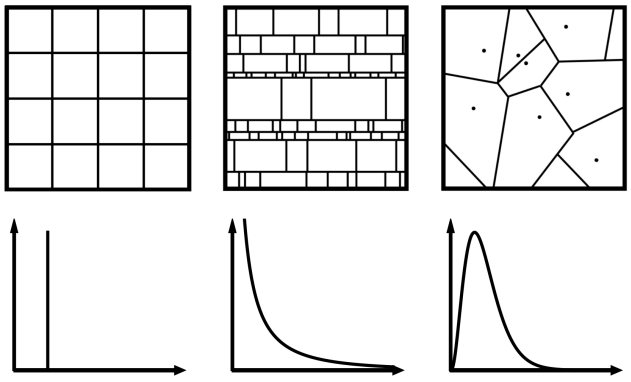

Figure 1: Visual comparison between three fragment area distributions corresponding to three distinct planar tessellations. From left to right: Dirac, Mott and Gamma distributions are observed.[12]

Mott pursued Lienau's work by studying the dynamic fragmentation of radially expanding cylindrical thin metal shells.[12] From experimental observations, he suggested that the cylinder

fragmentation followed two steps. First, a network of cracks parallel to the cylinder axis appears forming a set of strips of random width. Then, secondary crack networks appear in each strip along the cylinder axis forming the final fragments.

He considered the unidimensional Poisson-Voronoi distribution for modelling the intercrack spacing statistics and obtained the following estimate for the probability density function of the fragments area $a$:[12]

$$f(a) = \frac{\tau}{\sqrt{\tau a}} \int_0^\infty \left(2\xi\sqrt{\tau a} - 1\right)\left(1 + 1/\xi^2\right) \exp\left(-2\xi\sqrt{\tau a} - 1/\xi^2\right) \mathrm{d}\xi \tag{2}$$

where $\tau$ is the number of cracks in the cylinder per unit surface, i.e. the crack density.

While giving accurate estimates,[12,29] the distributions of Lienau and Mott do not consider the physics of fragmentation. As a consequence, the influence of a material parameter such as its elasticity modulus or its density on the fragments size distribution is still unknown at this point. The same goes with the influence of the boundary condition, in particular the influence of the loading speed on the crack density.

Aiming at filling this gap, Mott proposed a physical framework for modelling one-dimensional dynamic fragmentation problems under homogeneous strain state. He suggested the existence of a flaw population inside any solid, each flaw being associated to a particular critical strain value above which the flaw initiates a crack. As a consequence, release waves travel inside the body from the activated flaws locus preventing a future activation of any flaw they encounter.

The resulting number of activated flaw and thus the final crack density depends on the competition between the rate of released strain and the rate of increasing imposed strain. If the rate of imposed strain is low, only a few flaws are activated before the complete release of the solid. If the rate of imposed strain is high, a big part of the flaws are activated before the arrival of released waves, resulting in a higher final crack density.

Since, numerous *CDM* models have been proposed extending the use of Mott's theory for three-dimensional fragmentation problems involving inhomogeneous strain fields.[5,6,18–24] These models estimate crack density fields by means of finite element simulations.

Following the approach of Lienau and Mott, the crack density field can be used as an input of a partition algorithm. This algorithm would generate a representative partition of the fragmented solid, for example a Voronoi tessellation, which would in turn be used for estimating a fragment size distribution.

## 3 The Poisson-Voronoi tessellations

### 3.1 Homogeneous Poisson-Voronoi tessellations

A Voronoi partition of a domain $\Omega$ of size $|\Omega|$, associated to a set of $N$ points or seeds, splits $\Omega$ into $N$ Voronoi cells. Each Voronoi cell is associated to a seed and corresponds to the set of points inside $\Omega$ closer to that seed than to any other considering a given metric.

In this work we focus our interest into the homogeneous Poisson-Voronoi tessellations obtained by considering the euclidian metric. In these tessellations, the seeds are generated by a homogeneous Poisson point process over domain $\Omega$. Considering a point density $\lambda$, a number $N$ of seeds is randomly selected using a Poisson law with intensity $\lambda|\Omega|$. The $N$ seeds are then randomly placed inside $\Omega$ without preference for any spatial location and are used to build the Voronoi tessellation.

Consider a fragmented solid whose crack network corresponds exactly to the faces of a homogeneous Poisson-Voronoi tessellation. Consequently, the resulting fragments are identified to the Voronoi tessellation cells. The seed density $\lambda$ of the corresponding homogeneous Poisson-Voronoi tessellation is related to the face density, i.e. the crack density $\tau$, by:[30]

$$\lambda = \begin{cases} \left(\frac{1}{3}\right)\tau & \text{for planar tessellations} \\ \left(\frac{35}{35+24\pi^2}\right)\tau & \text{for volume tessellations} \end{cases} \tag{3}$$

The fragment or Voronoi cell size probability density function can be estimated by a Gamma distribution:[31]

$$\forall x \geq 0,\ f^H(d,\lambda;x) = \frac{x^{k(d)-1}}{\Gamma(k(d))}\,[k(d)\lambda]^{k(d)}\exp(-k(d)\lambda x) \tag{4}$$

where $\Gamma$ is the Euler Gamma function and $k$ is a positive scalar function depending only on the domain dimension $d$ and reading:

$$k(d) = \frac{3d+1}{2} \tag{5}$$

Accuracy of estimate (4) is illustrated on Figure 2.

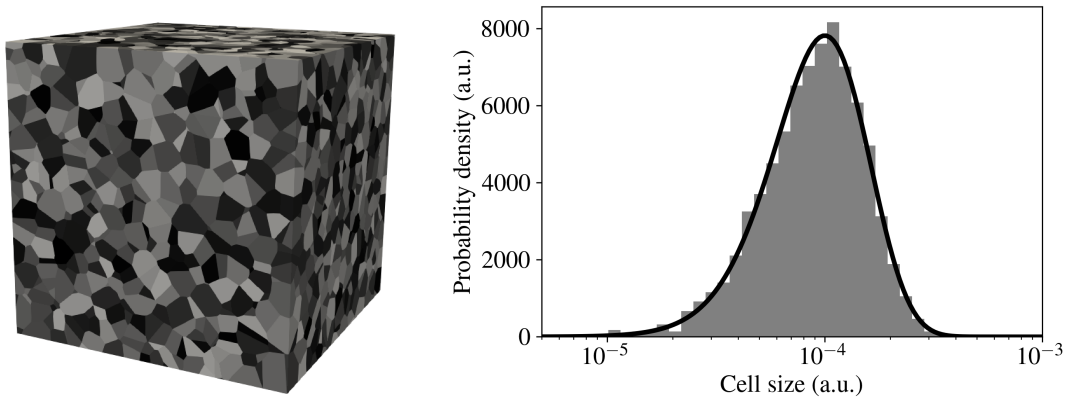


Figure 2: Left: a homogeneous Poisson-Voronoi tessellation of a cube. Right: the associated cell volume distribution (grey chart) and the proposed estimate (black line).

Equations (3), (4) and (5) can be used for estimating a fragment size distribution from a homogeneous crack density field defined over domain $\Omega$. For the estimate to be accurate, the fragmented solid should resemble a homogeneous Poisson-Voronoi tessellation. A first step for improving the representativity of the Voronoi tessellations is to allow for an inhomogeneous description of the crack density field.

### 3.2 Inhomogeneous Poisson-Voronoi tessellations

In most cases the crack density inside a solid is not homogeneous. In turn, it appears interesting to consider a Voronoi tessellation built on seeds drawned from an inhomogeneous Poisson point process. To the best of our knowledge, there are no known estimates for the probability density function of inhomogeneous Poisson-Voronoi tessellations.

Consider a solid occupying a domain $\Omega$ and an inhomogeneous crack density field $\tau$ defined over $\Omega$. Supposing that equation (3) still holds for inhomogeneous Poisson-Voronoi tessellations, the crack density field $\tau$ is substituted by its equivalent Voronoi cell density field $\lambda$:

$$\forall \bar{X} \in \Omega,\ \lambda(\bar{X}) = \begin{cases} \left(\frac{1}{3}\right) \tau(\bar{X}) & \text{for planar tessellations} \\ \left(\frac{35}{35+24\pi^2}\right) \tau(\bar{X}) & \text{for volume tessellations} \end{cases} \tag{6}$$

Let $\mathcal{F} = \lambda(\Omega)$ be the set of accessible values of $\lambda$ over domain $\Omega$. For all $x$ in $\mathcal{F}$, we define the cumulative domain size function $S$ by:

$$\forall x \in \mathcal{F},\ S(x) = |\left\{\bar{X} \in \Omega,\ \lambda(\bar{X}) \leq x\right\}| \tag{7}$$

By definition $S$ is a strictly increasing function hence injective. Denoting by $\mathcal{E}$ the image set of $\mathcal{F}$ through function $S$, we define the equivalent seed density $\lambda_{eq}$ as the reciprocal function of $S$:

$$\forall y = S(x) \in \mathcal{E},\ \lambda_{eq}(y) = x \tag{8}$$

The image set $\mathcal{E}$ is a disjoint union of singleton sets and non-singleton intervals:

$$\mathcal{E} = \bigsqcup_{k \in I} \{S_k\} \bigsqcup_{j \in J} \mathcal{E}_j \tag{9}$$

With the above notation and by using the total probability theorem, we estimate the Voronoi cell size probability density function $f^{NH}$ by the following equation:

$$\forall x \geq 0,\ f^{NH}(d;x) = \frac{1}{\Lambda} \left( \sum_{k \in I} f^H(d, \lambda_{eq}(S_k); x) \lambda_{eq}(S_k) S_k + \sum_{j \in J} \int_{\mathcal{E}_j} f^H(d, \lambda_{eq}(y); x) \lambda_{eq}(y) \mathrm{d}y \right) \tag{10}$$

where $\Lambda$ is the expected number of Voronoi cells inside $\Omega$:

$$\Lambda = \int_{\Omega} \lambda(\bar{X}) \mathrm{d}\Omega \tag{11}$$

Figure 3 illustrates the accuracy of estimate (10) on an example of inhomogeneous tessellation of a cube of side length $L$.

The seed density $\lambda$ considered on Figure 3 is defined over the cube by:

$$\forall (x,y,z) \in [0,L]^3,\ \lambda(x,y,z) = \left[ l_0 + (l_1 - l_0) \left( \frac{\max(x,y,z)^3}{L^3} \right) \right]^{-3} \tag{12}$$

where $l_0 = L/50$ and $l_1 = L/5$.

The associated crack density field $\tau$ is given by Equation (6). For all $v \in [0, L^3]$, the number $n(v)$ of cracks inside the cubic space $\mathcal{C}(v) = [0, v^{1/3}]^3$ is obtained by integrating the crack density field $\tau$ over $\mathcal{C}(v)$:

$$\forall v \in [0, L^3],\ n(v) = \left(1 + \frac{24\pi^2}{35}\right) \frac{L^3}{2\,(l_1 - l_0)\, l_0^2} \left[ 1 - \left( \frac{l_0}{l_0 + (l_1 - l_0) \left(\frac{v}{L^3}\right)} \right)^2 \right] \tag{13}$$

Figure 4 compares the expected cumulative crack number inside the cubes $\mathcal{C}(v)$ for $v \in [0, L^3]$ with the one corresponding to the Voronoi tessellation of Figure 3. Estimate (6) shows a relatively good accuracy.

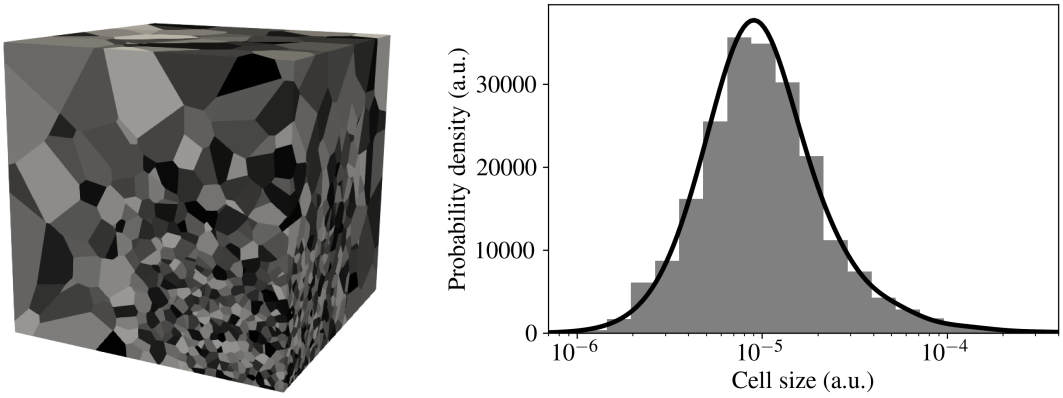


Figure 3: Left: an inhomogeneous Poisson-Voronoi tessellation of a cube generated with a thinning algorithm.[32] Right: the associated cell volume distribution (grey chart) and the proposed estimate (black line).

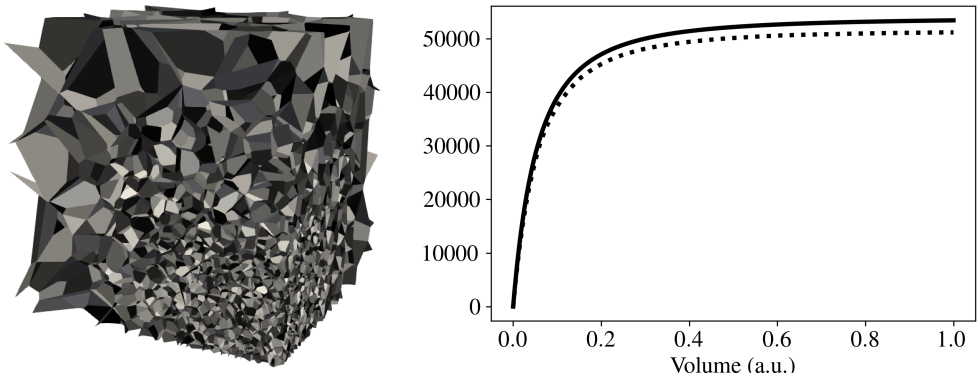


Figure 4: Left: cells faces network of an inhomogeneous Poisson-Voronoi tessellation of a cube. Right: the cumulative number of Voronoi cell faces inside cubes $\mathcal{C}(v)$, $v \in [0, L^3]$ (dotted line) and the proposed estimate (solid line).

A particular case concerns step crack density fields. Such fields are the usual output of numerous finite element simulations using damage models based on Mott's theory. Indeed, these simulations usually provide homogeneous crack density fields over each finite element. Denoting by $\lambda_k$ the seed density associated to the crack density $\tau_k$ inside element $k$ and by $S_k$ the size of element $k$, $k \in [\![1; N_e]\!]$, estimate (10) becomes:

$$\forall x \geq 0,\ f^{NH}(d; x) = \frac{\sum_{k=1}^{N_e} f^H(d, \lambda_k; x)\lambda_k S_k}{\sum_{k=1}^{N_e} \lambda_k S_k} \tag{14}$$

## 4 Application and limitation

### 4.1 Brittle fragmentation of a ceramic plate

In this subsection we consider the work of Forquin and Ando[33] on the fragmentation of *SPS-S* and *SPS-L* ceramic tiles ($60 \times 30 \times 8\ mm^3$) under edge-on-impact tests. In these tests, intense

fragmentations of ceramic tiles are induced by the impact of cylindrical steel projectiles on their edge (impact velocity of approximately 175 $m.s^{-1}$). A metalic casing surrounding the ceramic tiles limits the fragments displacement allowing for a postmortem observation of the fragmented tiles by microtomography.

Using the microtomographic pictures provided by Forquin and Ando,[33] a fragment density field has been estimated for the two types of tested ceramics by a trial and error approach. Inhomogeneous Poisson-Voronoi tessellations have then been built using these density fields and the corresponding cumulative mass distribution of the Voronoi cells have been computed and compared to experimental measurements. Figures 5 and 6 display the results of this study.

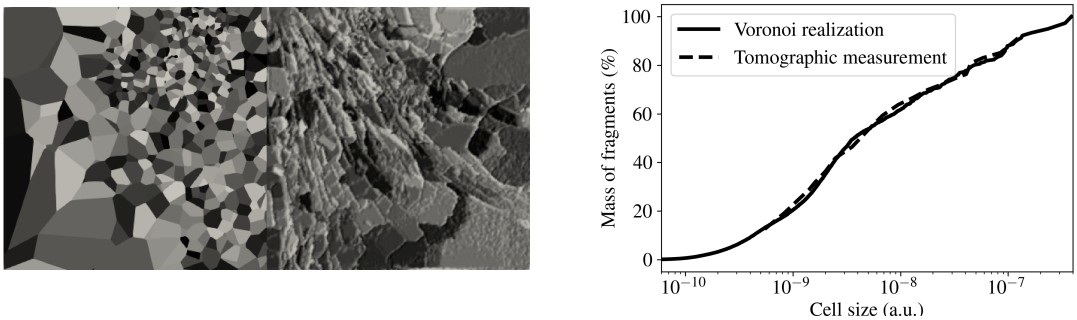


Figure 5: Left: a visual comparison between the tomographic picture of the fragmented *SPS-S* tile (right side) and a representative Poisson-Voronoi tessellation (left side). Right: comparison between the cumulative masses of the tile fragments and the Voronoi cell.

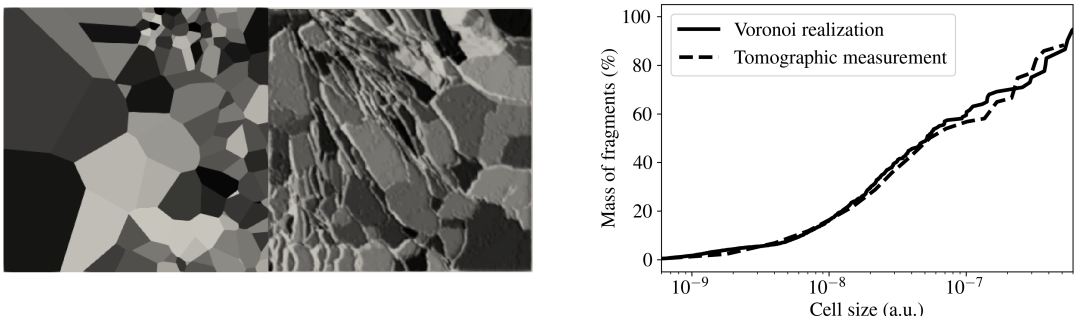


Figure 6: Left: a visual comparison between the tomographic picture of the fragmented *SPS-L* tile (right side) and a representative Poisson-Voronoi tessellation (left side). Right: comparison between the cumulative masses of the tile fragments and the Voronoi cell.

The use of inhomogeneous Poisson-Voronoi tessellations leads to accurate estimates of the cumulative mass distribution of the ceramic tiles fragments. In addition, the Voronoi tessellations allow for a qualitative observation of the fragmentation state over the tiles.

These encouraging results suggest that the inhomogeneous Poisson-Voronoi tessellation could be used for estimating a fragment size distribution given a crack density field inside a broken solid. Estimating the later seems to remain the main difficulty of the fragmentation problem.

### 4.2 The issue of apparent space dimension

Estimate (4) for the probability density function of the size of a homogeneous Poisson-Voronoi tessellation is accurate for describing unbounded Voronoi tessellations. In these tessellations, the statistics of the Voronoi cell geometrical features are only dependent on the space dimension $d$. The same statement can be made in the inhomogeneous case.

In turn, for the geometrical features statistics of the Voronoi cells to be representative of the expected ones in three-dimensional tessellations, the characteristic length $l_c$ of the Voronoi cells must remain neglectable with respect to all characteristic length of the broken plate. In particular it must be neglectable with respect to its thickness. This condition is writen in terms of the Voronoi cell density $\lambda$ and the plate thickness $l$ as follows:

$$\lambda >> l^{-3} \tag{15}$$

Figure 7 shows a tessellation of a thin plate associated to a Voronoi cell density which does not fullfil condition (15) and provides a visual comparison between the three-dimensional estimate for the Voronoi cell volume distribution and a "two-dimensional" one, hereafter denoted by $f_{2D}^H$.

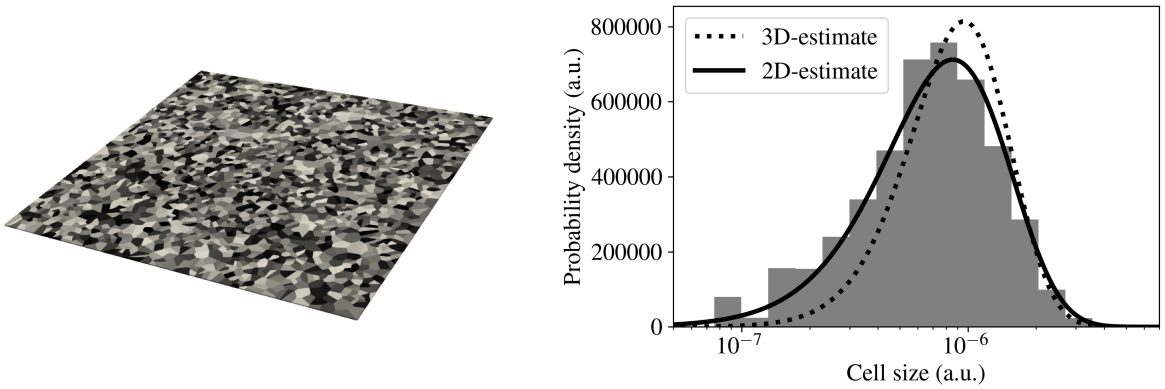


Figure 7: A homogeneous Poisson-Voronoi tessellation of a thin plate. On the left: The Voronoi cells. On the right: the Voronoi Cell size distribution (grey chart) and its estimates for three-dimensional fragmentation (dotted line) and two-dimensional fragmentation (solid line).

The two-dimensional distribution estimate $f_{2D}^H$ has been obtained by considering that each Voronoi cell is a cylinder whose thickness is equal to the plate one and having a cross section whose area distribution is given by estimate (4) for the two-dimenional case:

$$\forall x \geq 0,\ f_{2D}^H(\lambda; x) = \frac{1}{l} f^H(2, \lambda; \frac{x}{l}) \tag{16}$$

As illustrated on Figure 7, the use of estimate (16) rather than estimate (10) leads to a better approximation of the volume distribution of the Voronoi cells of the plate.

## 5 Conclusion

The use of isotropic inhomogeneous Poisson-Voronoi tessellations for representing fragmented solid has been investigated. Two formulas have been proposed and validated. The first one

estimates a Voronoi cell density field as function of a Voronoi face density field, i.e. the crack density field. The second one estimates the probability density function of the cell size of an isotropic inhomogeneous Poisson-Voronoi tessellation associated to a given cell density field. Although these formulas were known for homogeneous Poisson-Voronoi tessellations, to the best of our knowledge, their use had not previously been extended to inhomogeneous tessellations.

Knowing the crack density field inside a broken solid, these formulas can be used for obtaining a representative Voronoi tessellation of the solid and for providing an estimate of its fragment size distribution. A first application of these formulas for representing two broken ceramic tiles has been presented. The obtained Voronoi tessellations give good visual representations of the broken tiles. In addition, very good estimates of the cumulative fragment mass fraction of the ceramic tiles have been obtained. These results support the use of isotropic inhomogeneous Poisson-Voronoi tessellations for estimating the fragment size distribution of a fragmented brittle solid.

As showned in the last section of this paper, improvements can be made to address the usage limits of the proposed formulas for estimating fragment size distribution from a crack density fields. Others outlooks of this work concern the estimate of the crack density, which is here considered as an input data, and the enhancement of fragments geometric statistics description by considering anisotropic Voronoi tessellations. These future improvements should permit estimating fragments aspect ratio distribution, allowing for an estimation of fragments aerodynamic diameter distributions which are of crucial interest for assessments of health risks linked to exposure to fine particles.

## REFERENCES

[1] M. J. Steindler and W. B. Seefeldt. A Method for Estimating the Challenge to an Air-Cleaning System Resulting from an Accidental Explosive Event. In *Sixteenth Department of Energy Conference on Nuclear Air Cleaning*, 1980.

[2] DOE Handbook: Airborne Release Fractions/Rates and Respirable Fractions for NonReactor Nuclear Facilities. Volume I - Analysis of Experimental Data. Technical Report DOE-HDBK-3010-94, 1994.

[3] E. K. Garger, V. A. Kashpur, W. B. Li, and J. Tschiersch. Radioactive aerosols released from the Chernobyl Shelter into the immediate environment. *Radiation and Environmental Biophysics*, 45:105–114, 2006.

[4] O. Masson, W. Ringer, H. Mala, P. Rulik, M. Dlugosz-Lisiecka, K. Eleftheriadis, O. Meisenberg, A. De Vismes-Ott, and F. Gensdarmes. Size Distributions of Airborne Radionuclides from the Fukushima Nuclear Accident at Several Places in Europe. *Environmental Science & Technology*, 47:10995–11003, 2013.

[5] D. A. Shockey, D. R. Curran, L. Seaman, J. T. Rosenberg, and C. F. Petersen. Fragmentation of Rock under Dynamic Loads. *International Journal of Rock Mechanics and Mining Sciences & Geomechanics Abstracts*, 11(8):303–317, 1974.

[6] D. E. Grady and M. E. Kipp. Continuum Modelling of Explosive Fracture in Oil Shale. *International Journal of Rock Mechanics and Mining Sciences & Geomechanics Abstract*, 17:147–157, 1980.

[7] J. Aler, J. Du Mouza, and M. Arnould. Measurement of the fragmentation efficiency of rock mass blasting and its mining applications. *International Journal of Rock Mechanics and Mining Sciences & Geomechanics Abstracts*, 33(2):125–139, 1996.

[8] E. M. Kinyua, Z. Jianhua, R. M. Kasomo, D. Mauti, and J. Mwangangi. A review of the influence of blast fragmentation on downstream processing of metal ores. *Minerals Engineering*, 186(107743), 2022.

[9] R. G. O'Donnel. An investigation of the fragmentation behaviour of impacted ceramics. *Journal of Materials Science Letters*, 10:685–688, 1991.

[10] J.L. Zinszner, P. Forquin, and G. Rossiquet. Experimental and numerical analysis of the dynamic fragmentation in a SiC ceramic under impact. *International Journal of Impact Engineering*, 76:9–19, 2015.

[11] N. F. Mott. Fragmentation of shell cases. *Proceedings of the Royal Society A*, 189(1018):300–308, 1947.

[12] D. E. Grady. *Fragmentation of Rings and Shells: The Legacy of N. F. Mott.* Shock Wave and High Pressure Phenomena. Springer Berlin, Heidelberg, 2006.

[13] D. E. Grady and M. E. Kipp. Geometric statistics and dynamic fragmentation. *Journal of Applied Physics*, 58(3):1210–1222, 1985.

[14] P. Elek and J. Slobodan. Fragment Size Distribution in Dynamic Fragmentation: Geometric Probability Approach. *FME Transactions*, 36(2):59–65, 2008.

[15] N. Pourmoghaddam, M. A. Kraus, J. Schneider, and G. Siebert. The geometrical properties of random 2D Voronoi tesselations for the prediction of the tempered glass fracture pattern. *Special Issue: Engineered Transparency 2018 Glass in Architecture and Structural Engineering*, 2(5-6):325–339, 2018.

[16] L. F. Orozco, D.-H. Nguyen, J.-Y. Delenne, P. Sornay, and F. Radjai. Discrete-element simulations of comminution in rotating drums: Effects of grinding media. *Powder Technology*, 362:157–167, 2020.

[17] J. E. Bishop. Simulating the pervasive fracture of material and structures using randomly close packed Voronoi Tessellations. *Computational Mechanics*, 44:455–471, 2009.

[18] L. M. Taylor, E.-P. Cheng, and J. S. Kuszmaul. Microcrack-induced damage accumulation in brittle rock under dynamic loading. *Computer Method in Applied Mechanics and Engineering*, 55:301–320, 1986.

[19] B. J. Thorne, P. J. Hommert, and B. Brown. Experimental and computational investigation of the fundamental mechanics of cratering. In *International Symposium on Rock Fragmentation by Blasting*, Brisbane, 1990.

[20] L. Liu and P. D. Katsabanis. Development of a Continuum Damage Model for Blasting Analysis. *International Journal of Rock Mechanics and Mining Sciences*, 34(2):217–231, 1997.

[21] C. Denoual and F. Hild. A damage model for the dynamic fragmentation of brittle solids. *Computer Methods in Applied Mechanics and Engineering*, 183(3-4):247–258, 2000.

[22] P. Forquin and F. Hild. A probabilistic damage model of the dynamic fragmentation process in brittle materials. *Advances in Applied Mechanics*, 44:1–72, 2010.

[23] G. W. Ma, H. Hao, and F. Wang. Simulations of explosion-induced damage to underground rock chambers. *Journal of Rock Mechanics and Geotechnical Engineering*, 3(1):19–29, 2011.

[24] Z. Leng, Y. Fan, Q. Gao, and Y. Hu. Evaluation and optimization of blasting approaches to reducing oversize boulders and toes in open-pit mine. *International Journal of Mining Science and Technology*, 30:373–380, 2020.

[25] A. Burr, F. Hild, and F. A. Leckie. Micro-mechanics and continuum damage mechanics. *Archive of Applied Mechanics*, 65:437–456, 1995.

[26] Q. Du and D. Wang. Anisotropic Centroidal Voronoi Tessellations and their Applications. *SIAM Journal on Scientific Computing*, 26(3):737–761, 2005.

[27] T. F. W. Van Nuland, J. A. W. Van Dommelen, and M. G. D. Geers. An anisotropic Voronoi algorithm for generating polycrystalline microstructures with preferred growth directions. *Computational Materials Science*, 186:109947, 2021.

[28] D. R. Buckenberger, K. Buchin, and M. Botsch. Constructing $L_\infty$ Voronoi Diagrams in 2D and 3D. *Computer Graphics Forum*, 41(5):135–147, 2022.

[29] C. C. Lienau. Random fracture of a brittle solid. *Journal of the Franklin Institute*, 221(6):769–787, 1936.

[30] J. L. Meijering. Interface area, edge length, and number of vertices in crystal aggregates with random nucleation. *Philips Research Report*, 8:270–290, 1953.

[31] J.-S. Ferenc and Z. Néda. On the size distribution of Poisson Voronoi cells. *Physica A*, 385(2):518–526, 2007.

[32] P. A. W. Lewis and G. S. Shedler. Simulation of nonhomogeneous Poisson processes by thinning. *Naval Research Logistics Quarterly*, 26(3):377–551, 1979.

[33] P. Forquin and E. Ando. Application of microtomography and image analysis to the quantification of fragmentation in ceramics after impact loading. *Philosophical Transactions of the Royal Society A*, 375:20160166, 2017.